NANO LETTERS

2008
Vol. 8, No. 7
1896-1901

Strong Antimicrobial Coatings: Single-Walled Carbon Nanotubes Armored with Biopolymers

Dhriti Nepal,[†,‡] Shankar Balasubramanian,[†,§] Aleksandr L. Simonian,[§] and Virginia A. Davis*[,‡]

Department of Chemical Engineering and Materials Research and Education Center, Samuel Ginn College of Engineering, Auburn University, Auburn, Alabama 36849

Received February 22, 2008; Revised Manuscript Received April 29, 2008

ABSTRACT

Large scale biomimetic single-walled carbon nanotube (SWNT) coatings with significant antimicrobial activity, high Young's Modulus, and controlled morphology were fabricated using layer-by-layer assembly. Thickness was controlled within 1.6 nm and SWNT orientation was controlled using a directed air stream. This unique blend of multifunctionality and vertical and lateral control of a bottom-up assembly process is a significant advancement in developing macroscale assemblies with the combined attributes of SWNTs and natural materials.

Concern about the spread of infections through contact with contaminated surfaces was once limited to specific groups of people including astronauts who are subject to confined living spaces and the virulence-enhancing effects of space flight[1] and people requiring surgery or implantable devices.[2] More recently, there has been growing concern about the role of contaminated surfaces in the spread of infections such as severe acute respiratory syndrome (SARS),[3,4] and *Staphylococcus aureus*, particularly methicillin-resistant *Staphylococcus aureus* (MSRA).[5] Antimicrobial surfaces are therefore desirable not only for the aerospace, defense, and medical industries but also for the consumer product and public transportation industries. We have used layer-by-layer assembly to produce coatings that combine the strength of single-walled carbon nanotubes (SWNTs) with the antimicrobial activity of lysozyme (LSZ).

LSZ, a key member of ova-antimicrobials, is a powerful natural antibacterial protein.[6] It is in the class of enzymes which lyse the cell walls of Gram-positive bacteria by hydrolyzing the β-1,4 linkage between *N*-acetylmuramic acid (NAM) and *N*-acetylglucosamine (NAG) of gigantic polymers in the peptidoglycan (murein).[7,8] Unlike many antimicrobials, LSZ has both enzymatic and nonenzymatic activity in both its native and denatured states and is useful even in processes which require heat treatment. The potential use of LSZ as an antimicrobial agent in pharmaceuticals, food preservatives, and packaging is an active area of research,[7,8] but the effective use of LSZ requires incorporating it with a more mechanically robust material. SWNTs are well-known for exceptional combination of mechanical, electrical, thermal, and optical properties.[9–11] However, the efficient transfer of SWNTs' inherent nanoscale properties to macroscopic structures and devices has been an ongoing research challenge comprised of three main issues: SWNT dispersion, controlled assembly, and efficient load transfer. There has been growing interest in using biological materials to stabilize dispersions of pristine SWNTs. DNA enables much higher concentrations of dispersions of individual and small bundles of SWNTs[11,12] than any other known material besides superacids;[13,14] DNA−SWNT dispersions have even been used to produce liquid crystalline dispersions for solution spinning.[15] Similarly, favorable intermolecular interactions enable dispersion of individual and small bundles of SWNTs in proteins such as LSZ.[11,16,17] In this research, the strong Coulombic interactions between DNA and LSZ were exploited in the layer-by-layer (LBL) assembly[18–20] of DNA−SWNT and LSZ−SWNT dispersions.

The enzymatic activity of LSZ in the SWNT dispersions was determined by measuring the rate of lysis of Gram-positive *Micrococcus lysodeikticus* intact cells (Figure 1). The responses from the turbidimetric assay were modeled with first-order kinetics typically used to quantify exponential death of microorganisms (Figure 1b). The analysis shows that LSZ-SWNT dispersions clear approximately 55% of turbidity (optical density at 450 nm) within 5 min compared to 60% for the LSZ dispersion. The decrease in optical

* Corresponding author, davisva@auburn.edu.
† Authors contributed equally in this work.
‡ Department of Chemical Engineering.
§ Materials Research and Education Center.

10.1021/nl080522t CCC: $40.75
Published on Web 05/29/2008

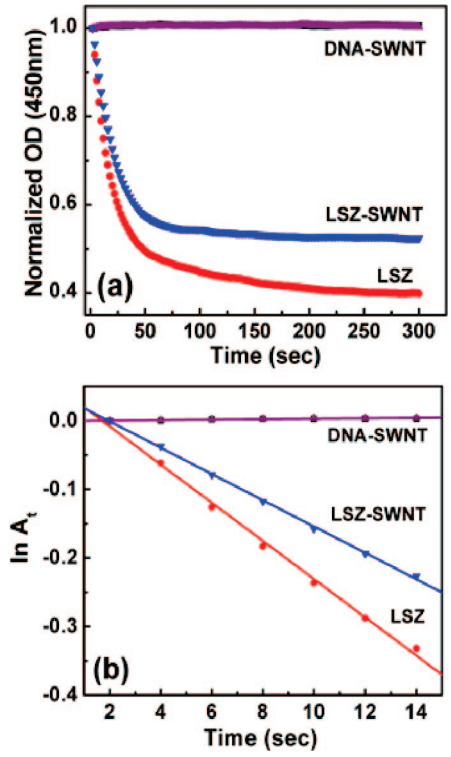

Figure 1. (a) Turbidimetric assay of LSZ and LSZ−SWNT conjugate in solution against *M. lysodeikticus*. (b) Rate of *M. lysodeikticus* lysis reaction (regression line is fit to the linear portion of experimental data points in (a) using first-order kinetics).

density due to cellular lysis confirms that secondary structure of LSZ in LSZ−SWNT conjugate is well preserved[16] as required for enzyme activity. In contrast, the DNA−SWNT dispersions showed no reduction in turbidity, suggesting that the SWNTs did not contribute to cell lysis.

Zeta potential measurements confirmed that the cationic and anionic nature of LSZ−SWNT (+22 mV) and DNA−SWNT dispersions (−30 mV) provided an excellent platform for strong electrostatic interaction between LSZ−SWNT and DNA−SWNT coatings $[(\text{LSZ}-\text{SWNT})-(\text{DNA}-\text{SWNT})]_n$. Secondary forces vital in DNA−protein interactions in biological systems, including van der Waals and $\pi-\pi$ attractions, were also likely to have played a significant role in interlayer adhesion. UV−vis−NIR absorption spectroscopy, ellipsometry, and surface plasmon resonance (SPR) were used in concert to monitor the growth of the LBL coatings on a variety substrates including silicon, gold, glass, and mica (Supporting Information). Absorbance spectroscopy (Figure 2a) showed well-resolved van Hove transitions of metallic (M_{11}) and semiconducting SWNTs (S_{11} and S_{22}), indicating that the SWNTs retained their electronic structure in the matrix and were predominantly dispersed as individual SWNTs.[10] The uniform increase of UV−vis−NIR absorbance from each deposition cycle revealed that film growth was linear and uniform. Moreover, ellipsometry showed a 1.6 nm (±0.03 nm) increase in thickness per layer; a value consistent with the previously reported diameter of individual DNA−SWNT adducts[21] (Figure 2b). Atomic force microscopy (AFM) provided further verification of deposition of

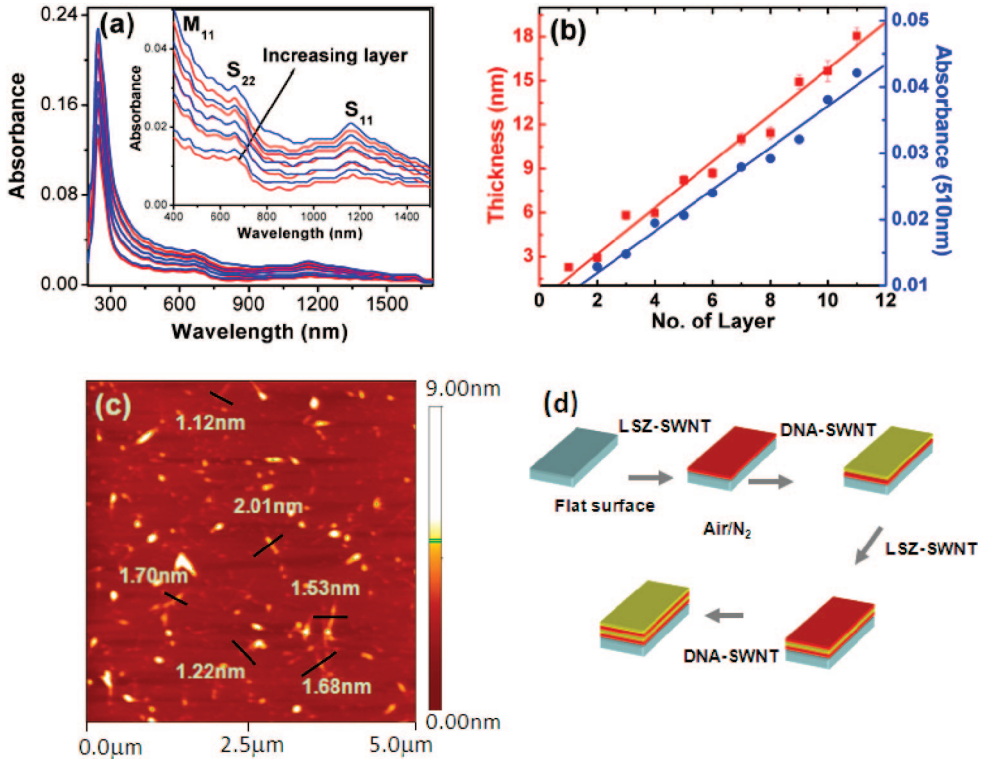

Figure 2. (a) UV−vis−NIR absorbance spectra of LBL assembly of LSZ−SWNT/DNA−SWNT (concentration of SWNT in dispersion ~25 mg/L). The inset magnifies the van Hove transitions of metallic and semiconducting SWNT. (b) Comparison of UV−vis accumulation curves for absorbance at 510 nm and ellipsometry thickness measurement of the LBL assembly. (c) AFM image of DNA−SWNT dried dispersion. (d) Schematic diagram of LBL assembly of LSZ−SWNT and DNA−SWNT.

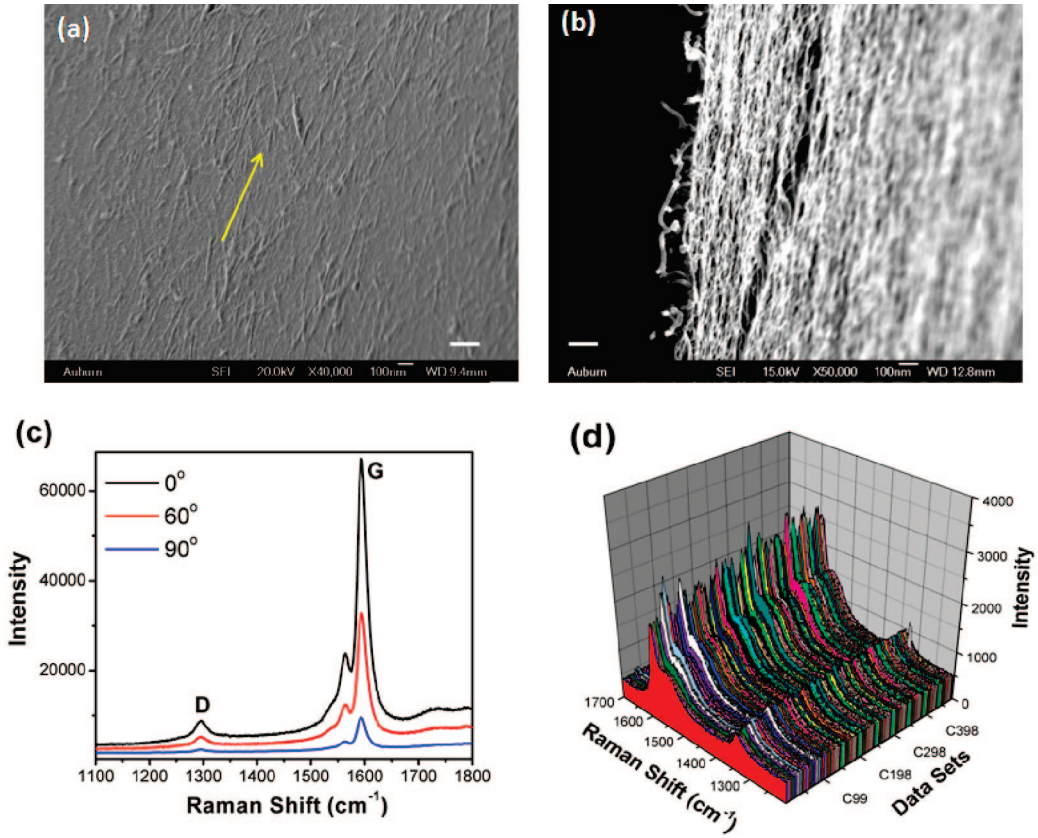

Figure 3. SEM images of LBL assembly of LSZ−SWNT/DNA−SWNT of the (a) 8th layer and (b) 68th layer. (c) Raman spectra of the assembly (eighth layer) showing D-band to G-band recorded at various angles between the polarization of laser excitation and SWNT alignment direction using a 514 nm laser. (d) Raman mapping collected at 10 × 10 μm area (eighth layer) showing D-band and G-band. The scale bars in (a) and (b) represent 200 nm.

individual SWNTs; the average diameters of the DNA−SWNT adducts (Figure 2c) was 1.6 nm. This extremely fine control of assembly process is the direct result of the quality of the initial dispersion.

SWNT orientation within each layer was achieved by applying a directed air stream between each deposition step. This step decreased the time required for assembly by eliminating the need for the rinsing step inherent in many LBL processes. Furthermore, the air stream enabled shear alignment of SWNTs within each individual layer generating the possibility to create coatings where each layer has a distinct orientation. Parts a and b of Figure 3 show scanning electron microscopy (SEM) images of the aligned 8th and 68th layers, respectively. Uniform deposition and alignment were further confirmed by Raman spectroscopy. Raman mapping was conducted to evaluate the spatial distribution of SWNT on the surface; G band intensities across a wide area (10 μm^2) are almost uniform showing that the SWNTs were uniformly spaced. It is well established that Raman intensity of SWNTs is maximal when exciting light polarization is along the nanotubes axis.[22–24] When the air stream was applied in random directions, no change in Raman intensity was observed indicating an isotropic orientation. However, directing the air stream in one direction resulted in a significant degree of alignment and a Raman ratio (G^0/G^{90}) of 7 (Figure 3c). The ability to align the SWNTs using a directed air stream is due to SWNTs rigid rod behavior in solution.[25,26] Shear-induced alignment of SWNTs has also been observed in films[27,28] and fibers.[29]

In order to better understand the LBL process, dispersions with different SWNT concentrations were produced with and without added electrolyte. SWNT concentration strongly influenced coating thickness. Figure 4 shows the UV−vis−NIR absorbance of LBL assembly from the 45 mg/L SWNT dispersion. The increasing intensity corresponds to increased SWNT concentration after the deposition of each layer (Figure 4a). The presence of clear van Hove peaks suggests that the SWNTs were predominantly individuals, but SEM revealed some small aggregates nonparallel overlapping SWNTs. Ellipsometry showed (Figure 4d) that increasing SWNT concentration from 25 to 45 mg/L increased the average layer thickness from 1.6 to 3.0 nm. The increased layer thickness at higher concentrations is believed to be largely due to SWNTs overlapping during the deposition process and perhaps an increase in the number of small bundles in the dispersion.

The addition of electrolyte also had an effect on the assembly process. Figure 4b shows the absorbance spectroscopy of LBL growth prepared in LSZ−SWNT and DNA−SWNT dispersions containing 45 mg/L SWNT and 10 mM NaCl. On each LSZ−SWNT layer, the rate of growth of absorbance is faster than that with DNA−SWNT. This corroborates with ellipsometry results (Figure 4e) and is further confirmed by surface plasmon resonance (SPR)

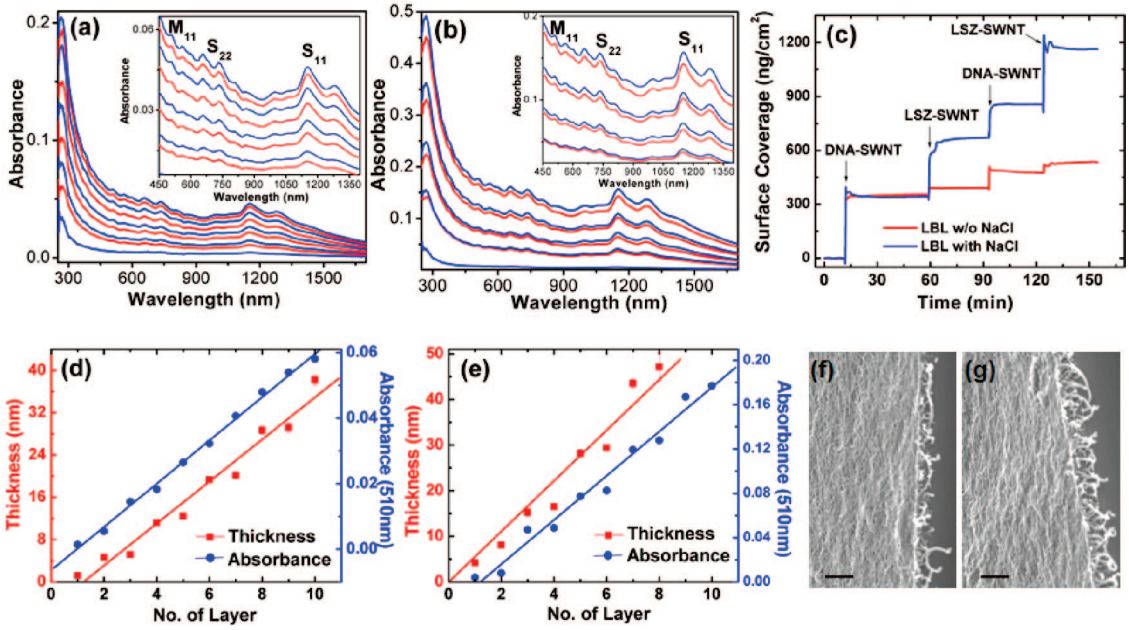

Figure 4. UV−vis−NIR absorbance spectra of LBL assembly of LSZ−SWNT/DNA−SWNT obtained from dispersion of SWNT at higher concentration (45 mg/L). Blue represents DNA−SWNT and red represents LSZ−SWNT (a) without NaCl and (b) with addition of NaCl (10 mM). The insets in (a) and (b) magnify the van Hove transitions of metallic and semiconducting SWNTs. (c) Surface plasmon resonance of in situ thin film deposition showing the surface coverage. Comparison of UV−vis accumulation curves for absorbance at 510 nm and ellipsometry thickness measurements of the LBL assembly from 45 mg/L SWNT dispersions (d) without NaCl and (e) with addition of NaCl (10 mM). (f and g) SEM images of the surface of the film (68th layer) without NaCl and with NaCl, respectively. The scale bars in (f) and (g) represent 200 nm.

spectroscopy, a surface sensitive technique which unambiguously demonstrates the effect of salt in LBL film assembly (Figure 4c). The rapid increase in SPR response provides strong evidence for electrostatic interactions between oppositely charged SWNT−bioadducts. SPR response increases smoothly over each layer indicating progressive assembly; surface coverage calculations indicate that more nanotubes were deposited in the presence of 10 mM NaCl. The influence of added salt[30] agrees well with reported values for similar SWNT−polyelectrolyte multilayers.[31–33] The presence of salt did not result in any obvious morphological differences in the coating after multiple deposition cycles (Figure 4, panels f and g).

Nanoindentation was used to determine the mechanical properties of 205 nm thick (68 layers) coatings. Figure 5 shows the hardness and Young's modulus as a function of penetration depth; the hardness was 1 GPa and the Young's modulus was 22 GPa. These results are similar to those measured by Mamedov et al.[34] and Xue et al.[35] and confirm effective load transfer between the SWNTs and the biomacromolecular matrix.

The enzymatic activities of the LBL coatings were evaluated as described in the Supporting Information. Remarkably, coatings terminating in a LSZ−SWNT layer exhibited a relative antimicrobial activity of 84% compared to 69% in the initial dispersion (Figure 6). The clearing of the turbid *M. lysodeikticus* solution by the coatings is due to the enzyme activity of the exposed LSZ−SWNT layer suggesting a dynamic interaction between the coating surface and the surrounding solution. It is important to note that no lytic activity was observed for surface layers ending with

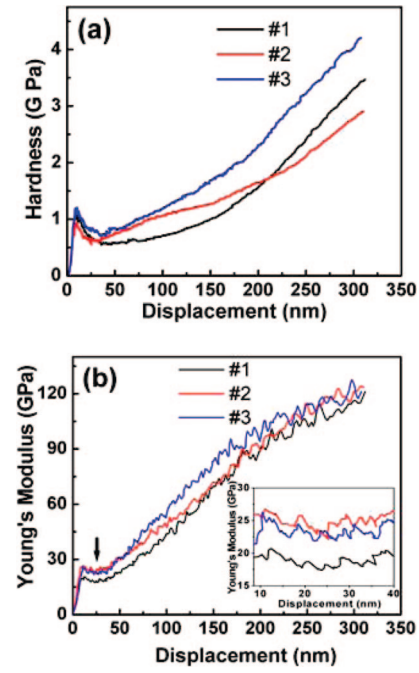

Figure 5. Nanoindentation tests on a 68 layer coating (LSZ−SWNT/DNA−SWNT)$_{68}$ of (a) hardness and (b) Young's modulus. The inset in (b) shows the plateau region where Young's modulus was calculated.

DNA−SWNT or unmodified surfaces (Student's *t* test, $P < 0.05$). This confirms that the antimicrobial activity was specifically due to the LSZ enzyme reaction and not the presence of SWNTs. Of particular interest is that the number of layers has an influence on the antimicrobial activity of the coating (Figure 6b). This behavior suggests that a zone-

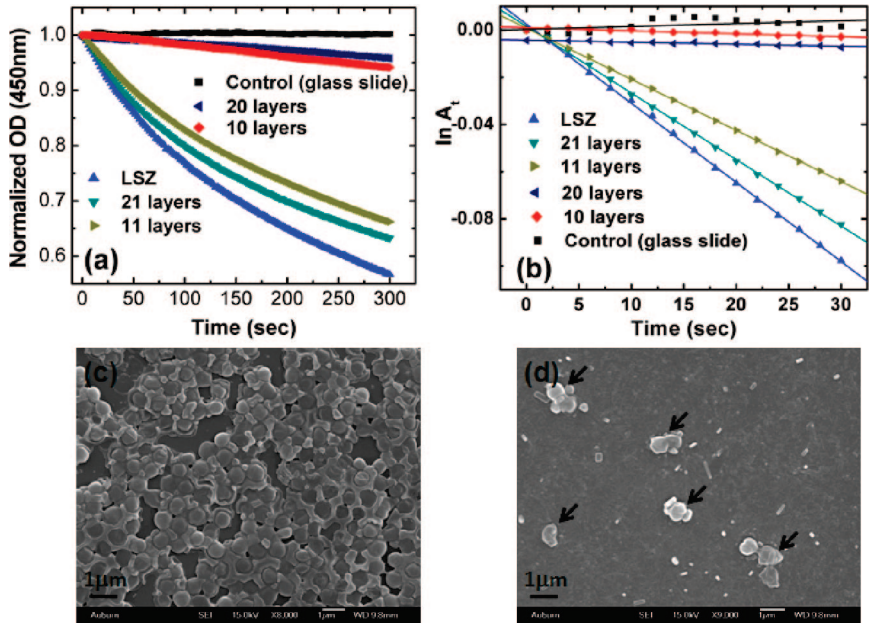

Figure 6. (a) Effect of different layers of LBL coating against *M. lysodeikticus* in turbidimetric assay. (b) Rate of *M. lysodeikticus* lysis reaction (regression line is fit to the linear portion of experimental data in (a) using first-order rate kinetics). SEM image of samples incubated with *Staphylococcus aureus* at 37 °C for 24 h of (c) a clean silicon wafer (control) and (d) LBL assembly at 11th layer (top surface LSZ−SWNT) arrows indicating damaged cells). The scale bars in (c) and (d) represent 1 μm.

model behavior is observed as outlined by Ladam et al.[36] where the substrate affects the growth of initial layers forming zone I followed by growth of zone II and zone III as the number of layers increased. On the other hand, this may also arise from interplay of charges during film growth as the underlying layers are overcompensated compared to terminal layers.[37] This unequal distribution of charges on different layers may influence the activity of LSZ since it must have an optimal balance of charges in order to express lytic activity.[8] The coatings exhibited impressive long-term stability; no leaching of enzyme was observed in the supernatant when the coatings were stored in buffer and the antimicrobial activity is retained for at least 60 days (see Supporting Information).

Exposing surfaces to freshly prepared *Staphylococcus aureus* provided further evidence of the antimicrobial activity of LSZ−SWNT terminated coatings. When silicon substrates with and without the LBL assembled coating were incubated with *Staphylococcus aureus* for 24 h at 37 °C and imaged under SEM, significantly more bacteria adhered to the uncoated (Figure 6c) surface than to the coated surface (Figure 6d). In addition, the few bacteria that adhered to the coated substrate underwent severe morphological changes. In contrast, on the uncoated silicon surface the cells remained intact and maintained their cocci structure. These morphological changes in *Staphylococcus aureus* cells are speculated to be the result of lysozyme triggered autolysis of bacteria which is the generally accepted mechanism of lysozyme action on *Staphylococcus aureus* cells.[38,39]

In conclusion, we have developed a unique multifunctional biomimetic material comprised of SWNT, DNA, and LSZ using LBL assembly. Precise control of both layer thickness and SWNT alignment within each layer was achieved, and the final coatings had robust mechanical properties. Coatings ending in an exposed LSZ−SWNT layer exhibit excellent long-term antimicrobial activity. This has several distinct advantages over coatings which release antimicrobials over time; controlled release coatings lose their antimicrobial efficiency once the concentration of the antimicrobial agent drops below the minimum inhibitory concentration (MIC). On the other hand, our nonleaching coatings exhibit robust mechanical properties and long-term protection against bacterial colonization. Furthermore, the spectrum of disinfection of LSZ−SWNT layers can be extended to Gram-negative bacteria by simply including chelators such as EDTA.[8] The results of this research demonstrate the significant possibilities for the molecular design of hybrid structural materials from SWNTs and natural biopolymers. Such robust, antimicrobial materials have significant promise in applications including medicine, aerospace engineering, public transportation, home appliances, and sporting goods.

Acknowledgment. This research was supported by National Science Foundation Grant (CTS-0330189) and USDA-CSREES Grant (2006-34394-16953). The authors acknowledge Vinod Radhakrishnan and Matthew Kayatin for Raman spectrum, Shanthi Murali for atomic force microscopy, Dr. Barton C. Prorok and Bo Zhou for nanoindentation, and Subasri Ayyadurai (University of Cincinnati) for zeta potential measurements. The authors thank the Richard E. Smalley Institute for Nanoscale Science and Technology for providing SWNTs.

Supporting Information Available: Experimental details and additional information on antimicrobial activity. This material is available free of charge via the Internet at http://pubs.acs.org.

References

(1) Wilson, J. W.; Ott, C. M.; zu Bentrup, K. H.; Ramamurthy, R.; Quick, L.; Porwollik, S.; Cheng, P.; McClelland, M.; Tsaprailis, G.; Radabaugh, T.; Hunt, A.; Fernandez, D.; Richter, E.; Shah, M.; Kilcoyne, M.; Joshi, L.; Nelman-Gonzalez, M.; Hing, S.; Parra, M.; Dumars, P.; Norwood, K.; Bober, R.; Devich, J.; Ruggles, A.; Goulart, C.; Rupert, M.; Stodieck, L.; Stafford, P.; Catella, L.; Schurr, M. J.; Buchanan, K.; Morici, L.; McCracken, J.; Allen, P.; Baker-Coleman, C.; Hammond, T.; Vogel, J.; Nelson, R.; Pierson, D. L.; Stefanyshyn-Piper, H. M.; Nickerson, C. A. *Proc. Natl. Acad. Sci.U.S.A.* **2007**, *104*, 16299–16304.

(2) Darouiche, R. O. *N. Engl. J. Med.* **2004**, *350*, 1422–1429.

(3) Cheng, V. C. C.; Lau, S. K. P.; Woo, P. C. Y.; Yuen, K. Y. *Proc. Natl. Acad. Sci.U.S.A.* **2007**, *20*, 660–694.

(4) Chu, C.-M.; Cheng, V. C. C.; Hung, I. F. N.; Chan, K.-S.; Tang, B. S. F.; Tsang, T. H. F.; Chan, K.-H.; Yuen, K.-Y. *Emerging Infect. Dis.* **2005**, *11*, 1882–1886.

(5) Klevens, R. M.; Morrison, M. A.; Nadle, J.; Petit, S.; Gershman, K.; Ray, S.; Harrison, L. H.; Lynfield, R.; Dumyati, G.; Townes, J. M.; Craig, A. S.; Zell, E. R.; Fosheim, G. E.; McDougal, L. K.; Carey, R. B.; Fridkin, S. K. *JAMA, J. Am. Med. Assoc.* **2007**, *298*, 1763–1771.

(6) Jolles, J.; Jolles, P. *Mol. Cell. Biochem.* **1984**, *63*, 165–189.

(7) Proctor, V. A.; Cunningham, F. E. *Crit. Rev. Food Sci. Nutr.* **1988**, *26*, 359–395.

(8) Losso, J.; Nakai, S.; Charter, E. In *Natural Food Antimicrobial Systems*; Naidu, A. S., Ed.; CRS Press: Boca Raton, FL, 2000; pp 185−210..

(9) Huang, J. Y.; Chen, S.; Wang, Z. Q.; Kempa, K.; Wang, Y. M.; Jo, S. H.; Chen, G.; Dresselhaus, M. S.; Ren, Z. F. *Nature* **2006**, *439*, 281–281.

(10) O'Connell, M. J.; Bachilo, S. M.; Huffman, C. B.; Moore, V. C.; Strano, M. S.; Haroz, E. H.; Rialon, K. L.; Boul, P. J.; Noon, W. H.; Kittrell, C.; Ma, J.; Hauge, R. H.; Weisman, R. B.; Smalley, R. E. *Science* **2002**, *297*, 593–596.

(11) Nepal, D.; Geckeler, K. E. In *Functionalization of Carbon Nanotubes*; Geckeler, K. E., Rosenberg, E., Eds.; American Scientific Publishers: Valencia, CA, 2006; pp 57–79.

(12) Nepal, D.; Sohn, J.-I.; Aicher, W. K.; Lee, S.; Geckeler, K. E. *Biomacromolecules* **2005**, *6*, 2919–2922.

(13) Davis, V. A.; Ericson, L. M.; Parra-Vasquez, A. N.; Fan, H.; Wang, Y.; Prieto, V.; Longoria, J. A.; Ramesh, S.; Saini, R.; Kittrell, C.; Billups, W. E.; Adams, W. W.; Hauge, R. H.; Smalley, R. E.; Pasquali, M. *Macromolecules* **2004**, *37*, 154–160.

(14) Rai, P. K.; Pinnick, R. A.; Parra-Vasquez, A. N. G.; Davis, V. A.; Schmidt, H. K.; Hauge, R. H.; Smalley, R. E.; Pasquali, M. *J. Am. Chem. Soc.* **2006**, *128*, 591–595.

(15) Barisci, J. N.; Tahhan, M.; Wallace, G. G.; Badaire, S.; Vaugien, T.; Maugey, M.; Poulin, P. *Adv. Funct. Mater.* **2004**, *14*, 133–138.

(16) Nepal, D.; Geckeler, K. E. *Small* **2006**, *2*, 406–412.

(17) Nepal, D.; Geckeler, K. E. *Small* **2007**, *3*, 1259–1265.

(18) Hammond, P. T. *Curr. Opin. Colloid Interface Sci.* **1999**, *4*, 430–442.

(19) Tang, Z.; Wang, Y.; Podsiadlo, P.; Kotov, N. A. *Adv. Mater.* **2006**, *18*, 3203–3224.

(20) Jiang, C.; Tsukruk, V. V. *Adv. Mater.* **2006**, *18*, 829–840.

(21) Zheng, M.; Jagota, A.; Semke, E. D.; Diner, B. A.; Mclean, R. S.; Lustig, S. R.; Richardson, R. E.; Tassi, N. G. *Nat. Mater.* **2003**, *2*, 338–342.

(22) Jorio, A.; Dresselhaus, G.; Dresselhaus, M. S.; Souza, M.; Dantas, M. S. S.; Pimenta, M. A.; Rao, A. M.; Saito, R.; Liu, C.; Cheng, H. M. *Phys. Rev. Lett.* **2000**, *85*, 2617.

(23) Ericson, L. M.; Fan, H.; Peng, H.; Davis, V. A.; Zhou, W.; Sulpizio, J.; Wang, Y.; Booker, R.; Vavro, J.; Guthy, C.; Parra-Vasquez, A. N. G.; Kim, M. J.; Ramesh, S.; Saini, R. K.; Kittrell, C.; Lavin, G.; Schmidt, H.; Adams, W. W.; Billups, W. E.; Pasquali, M.; Hwang, W.-F.; Hauge, R. H.; Fischer, J. E.; Smalley, R. E. *Science* **2004**, *305*, 1447–1450.

(24) Chae, H. G.; Minus, M. L.; Kumar, S. *Polymer* **2006**, *47*, 3494–3504.

(25) Doi, M.; Edwards, S. F. *The Theory of Polymer Dynamics*; Oxford University Press; Oxford, 1986.

(26) Duggal, R.; Pasquali, M. *Phys. Rev. Lett.* **2006**, 96.

(27) Shim, B. S.; Kotov, N. A. *Langmuir* **2005**, *21*, 9381–9385.

(28) Hedberg, J.; Dong, L.; Jiao, J. *Appl. Phys. Lett.* **2005**, *86*, 143111–3.

(29) Davis, V. A.; Pasquali, M. In *Nanoengineering of Structural, Functional and Smart Materials*; Schulz, M. J., Kelkar, A., Sundaresan, M. J., Eds.; CRC Press: Boca Raton, FL, 2005.

(30) Hofmeister, F. *Arch. Exp. Pathol. Pharmakol.* **1888**, *24*, 247–260.

(31) Paloniemi, H.; Lukkarinen, M.; Aaritalo, T.; Areva, S.; Leiro, J.; Heinonen, M.; Haapakka, K.; Lukkari, J. *Langmuir* **2006**, *22*, 74–83.

(32) Kovtyukhova, N. I.; Mallouk, T. E. *J. Phys. Chem. B* **2005**, *109*, 2540–2545.

(33) Rouse, J. H.; Lillehei, P. T.; Sanderson, J.; Siochi, E. J. *Langmuir* **2004**, *16*, 3904–3910.

(34) Mamedov, A. A.; Kotov, N. A.; Prato, M.; Guldi, D. M.; Wicksted, J. P.; Hirsch, A. *Nat. Mater.* **2002**, *1*, 190–194.

(35) Xue, W.; Cui, T. *Nanotechnology* **2007**, *18*, 145709.

(36) Ladam, G.; Schaad, P.; Voegel, J. C.; Schaaf, P.; Decher, G.; Cuisinier, F. *Langmuir* **2000**, *16*, 1249–1255.

(37) Schwarz, B.; Schonhoff, M. *Colloids Surf., A* **2002**, *198−200*, 293–304.

(38) Virgilio, R.; Gonzalez, C.; Munoz, N.; Mendoza, S. *J. Bacteriol.* **1966**, *91*, 2018–2024.

(39) Wecke, J.; Lahav, M.; Ginsburg, I.; Giesbrecht, P. *Arch. Microbiol.* **1982**, *131*, 116–123.

NL080522T